Novel Fe–Ni–Graphene composite electrode for hydrogen production

Article *in* International Journal of Hydrogen Energy · September 2015

DOI: 10.1016/j.ijhydene.2015.06.040

CITATIONS
89

READS
490

5 authors, including:

Subramanya Badrayyana
Indian Institute of Technology Bombay
11 PUBLICATIONS **597** CITATIONS

SEE PROFILE

A. Chitharanjan Hegde
National Institute of Technology Karnataka
118 PUBLICATIONS **2,254** CITATIONS

SEE PROFILE

Available online at www.sciencedirect.com

ScienceDirect

journal homepage: www.elsevier.com/locate/he

Novel Fe–Ni-Graphene composite electrode for hydrogen production

Subramanya Badrayyana, Denthaje Krishna Bhat, Sandhya Shenoy, Yathish Ullal, Ampar Chitharanjan Hegde*

Department of Chemistry, National Institute of Technology Karnataka, Surathkal, Mangalore 575 025, India

ARTICLE INFO

Article history:
Received 14 February 2015
Received in revised form
5 June 2015
Accepted 9 June 2015
Available online 4 July 2015

Keywords:
Electrodeposition
Electrocatalyst
Hydrogen evolution reaction
Graphene
Composite coating

ABSTRACT

We have developed a novel, efficient and economical composite electrode for hydrogen production. The electrode has been formed by embedding graphene in the Fe–Ni matrix via room temperature electrodeposition. The obtained active coatings have been tested for their efficiency and performance as electrode surfaces for hydrogen evolution reaction (HER) in 6 M KOH by cyclic voltammetry and chronopotentiometry techniques. The coating obtained at 60 mA cm^{-2} exhibited approximately 3 times higher activity for hydrogen production than that of binary Fe–Ni alloy. Addition of graphene to electrolyte bath resulted in porous 3D projections of nano-sized spheres of Fe–Ni on the surface of graphene, which effectively increased the electrochemically active surface area. XPS analysis results showed the equal distribution of both Ni metal and NiO active sites on the composite. The addition of graphene favoured the deposition of metallic nickel, which accelerated the rate determining proton discharge reaction. All these factors remarkably enhanced the HER activity of Fe–Ni-Graphene (Fe–Ni-G) composite electrode. The Tafel slope analysis showed that the HER follows Volmer-Tafel mechanism. The structure –property relationship of Fe–Ni-G coating has been discussed by interpreting field emission scanning electron microscopy (FESEM), X-ray photoelectron spectroscopy (XPS) and X-ray diffraction (XRD) analysis results.

Introduction

It is estimated that global energy demand for a sustainable development will double by 2050 [1]. This has necessitated a quest for reliable energy sources. Hydrogen is predicted to be a promising secondary energy, with the advantage of high energy density (140 MJ kg^{-1}) which far exceeds that of gasoline and coal, no carbon emission and a useful by-product of water from combustion [2,3]. Hydrogen, the first element of modern periodic table, exists as H_2 gas in nature in negligible amount whereas most of hydrogen is existing in fused state with oxygen as H_2O, which occupies about 70% of earth. The easiest and safest way to obtain high purity H_2 gas from water is by electrolysis [4–6]. The mechanism for HER is widely accepted to take place via two steps; initiation of reaction with a proton discharge to give adsorbed hydrogen atom, Volmer reaction (Eq. (1)),

$$H_2O + M + e^- \rightleftharpoons MH_{ads} + OH^- \quad (1)$$

* *Corresponding author.*
E-mail addresses: denthajekb@gmail.com, kishan@nitk.edu.in (D.K. Bhat).
http://dx.doi.org/10.1016/j.ijhydene.2015.06.040

It is followed either by Tafel reaction (Eq. (2)) where two adsorbed H atoms recombine to yield hydrogen or Hevrosky reaction (Eq. (3)) where an electrodesorption step takes place yielding hydrogen gas [7].

$$2\,MH_{ads} \rightleftharpoons 2M + H_2\uparrow \quad (2)$$

$$MH_{ads} + H_2O + e^- \rightleftharpoons M + OH^- + H_2\uparrow \quad (3)$$

The use of electrolytic devices to produce hydrogen is generally linked to its energetic properties or commercial interests [6]. In any industrial electrolyzers, the electrode materials are the most important components. The prerequisites for a material to qualify as electrode material for water electrolysis are high surface area, maximum electrical conductance, corrosion resistance in operating medium and good electrocatalytic property with minimum overvoltage [8,9]. Platinum shows very high activity for HER but its cost is very high [10]. Mo and W based HER electrocatalysts are active but they are not very abundant [11,12]. The best electrode materials for HER must constitute strong intrinsic catalytic activity, large surface area, stability of performance, availability in abundance and low cost [13]. Thus, in recent years the investigations on developing new, cheaper materials and improving existing materials for water electrolysis to obtain high purity hydrogen gas has gained considerable attention among researchers. The first row transition metals like Fe, Co and Ni are cheaper, abundant and have the potential to be better electrocatalysts [7,14–17]. A good number of reports pertaining to HER studies employing these metals and their alloys prepared by different techniques like mechanical alloying [18–20], sputtering [21], thermo-chemical [22] and electrodeposition [23–25] are available in the literature.

Recently the electrodeposition and electrocatalytic activity of Fe–Ni alloy coating was reported by our research group [26]. The composite electrodes of transition metal alloys for HER are gaining prominence in recent years due to their low cost, high stability and excellent electrocatalytic activity [27,28]. Materials like TiO_2, RuO, MoO_2, tungsten carbide and carbon nanopowder are used in combination with transition metals to enhance their electrocatalytic behaviour and stability [29–35]. Recently, interesting findings on the effect of embedded carbon content in Fe–Ni electrodes for HER in seawater were reported [36,37]. The presence of carbon content was found to be beneficial in enhancing the electrocatalytic property of the material.

On the other hand, graphene, the 2D form of carbon, has gained great scientific consideration in recent years due to its extraordinary electronic and mechanical properties like high mobility of charge carriers, high thermal conductivity, high mechanical strength, extremely large surface area, etc. [38–40]. These noteworthy properties of graphene make it well suited for many applications such as graphene-based electronics, composite materials, molecular gas sensors, energy storage and conversion [40–44]. Graphene, as defined, is a single layer two-dimensional material, comprising of carbon atoms arranged in a hexagonal manner, but graphene samples with two layers (bi-layer graphene) and more than two but less than ten layers (few-layer graphene) are equally of interest.

In view of the aforesaid aspects and as a part of our ongoing research on synthesis and applications of graphene [45,46] we thought it is worthwhile to investigate HER properties of transition metal alloy-graphene composite electrode. Accordingly we report herein the fabrication of a novel electrodeposited Fe–Ni-G composite electrode and studies on its performance as cathode for HER. The study was aimed at combining the high surface area of graphene with electrocatalytic property of Fe–Ni alloy to obtain hybrid porous electrodes from a single step electrodeposition. The porosity of non-precious metal electrocatalysts is increased mainly by leaching out certain metals from electrodeposited coatings to impart porosity to the surface [47,48]. The present single step electrodeposition method eliminates requirement of the post treatment of electrodeposited samples and hence they can be directly used for HER. We have carried out the electrodeposition of nanocrystalline Fe–Ni-G composite coating and have studied their applicability to HER or water splitting reaction in alkaline medium. Further, we have investigated the effect of graphene on electrocatalytic and physical properties of the coatings systematically and the observed results are discussed in the following sections.

Materials and methods

Electrodeposition of Fe–Ni-G composite coating

The electrodeposition of Fe–Ni-G electrocatalyst was accomplished in an acid sulphate bath with composition and operating parameters as given in Table 1. Fe–Ni-G composite coatings were deposited on a cross sectional area of copper rod using a customized glass cell. Mirror polished copper surface (exposed area of 1.0 cm^2) was electro-cleaned and then pickled in a mixture of 0.5 M HNO_3 and 0.5 M H_2SO_4 to activate the surface. Pure Ni plate with equal exposed surface area was used as an anode. The cathode and anode were placed parallel at 5 cm distance during plating. 0.5 g L^{-1} of synthesized graphene (S1 Supporting Information) was added into Fe–Ni bath. The bath was then agitated ultrasonically for 48 h to ensure uniform dispersion of graphene. Agilent N6705A DC power analyser was used as a high sensitive power source for electrodeposition. The total time for electrodeposition was fixed at 900 s in all the cases. To compare the electrocatalytic properties of Fe–Ni-G electrode with Fe–Ni coatings we have carried out the electrodeposition of Fe–Ni

Table 1 – Composition and operating parameters for deposition of Fe–Ni-G composite coatings on copper substrate.

Composition	Concentration (g L^{-1})	Operating parameter
$NiSO_4.6H_2O$	100	Cathode: Pure Cu
$FeSO_4.7H_2O$	25	Anode: Pure Ni
Boric acid	20	Temperature: 303 K
Ascorbic acid	5	pH: 3.5
Sodium lauryl sulfate	1	Current density: 20–60 mA cm^{-2}

0.5 g L^{-1} of synthesized graphene was added to obtain Fe–Ni-G composite coatings.

alloy on copper substrate and characterized as per the reported procedure [26].

Characterization

The surface morphology of electrodeposited coatings were characterized by field emission scanning electron microscope (FESEM) using Zeiss Ultra 55 field emission scanning electron microscope. The elemental composition and phase structures were analysed using X-ray photoelectron spectroscopy (XPS) taken on an AXIS Ultra instrument from Kratos Analytical in the range of 1–1300 eV and X-ray diffraction (XRD) measurements were conducted using a D8 Advance (Bruker) X-ray diffractometer with Cu Kα radiation (λ = 1.5418 Å). Electrocatalytic study of Fe–Ni alloy and Fe–Ni-G composite coatings were carried out using a custom made three-electrode tubular glass cell, with arrangements as shown in Fig. 1.

The electrochemical cell was designed for quantitative measurement of hydrogen, where electrodeposited Fe–Ni-G composite electrode was subjected to cathodic and anodic polarization, respectively. Electrodeposited Fe–Ni-G composite coating obtained under different deposition conditions was used as the test electrode with platinised platinum of same surface area (1.0 cm^2) as the counter electrode and saturated calomel electrode (SCE) as the reference electrode. All potentials reported in the present study are with reference to SCE. Luggin's capillary with agar-KCl salt bridge was used to minimize the error due to Ohmic drop.

Electrochemical behaviour of the coatings, in terms of HER, were evaluated by subjecting it to cyclic voltammetry and chrono-potentiometry studies in 6 M KOH medium, using computer controlled potentiostat VersaStat3-400 (Princeton Applied Research, USA). The cell was fitted with a graduated gas collector where the liberated hydrogen replaces corresponding amount of solution. This facility allows relating the amount of gas liberated at given time for electrode materials deposited at a given current density.

Results and discussion

The composition and operating parameters of the bath used for deposition of Fe–Ni-G composite in the present study is given in Table 1. The plating parameters and bath composition used were optimized by standard Hull cell method described elsewhere [1]. Fe–Ni-G composite coatings have been deposited on cross sectional area of copper rod using customised glass cell at different current densities (i) i.e., 20, 40 and 60 mA cm^{-2}. The deposits were analysed for surface morphology and compositional variation with applied current density.

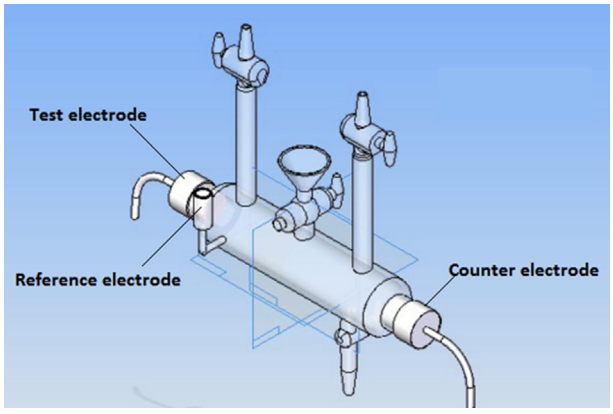

Fig. 1 – Customised tubular 3-electrode cell with provision to collect liberated H_2 on the electrode surface.

Surface and compositional characterization

FESEM analysis

Electrocatalysis is a heterogeneous process and is a function of surface morphology of the electrode material. The accepted mechanism for HER proceeds through an adsorption step basically [49–53]. Hence it is the surface structure and morphology that is vital in electrocatalytic materials developed by electrodeposition. The structure and morphology of Fe–Ni alloy coating surfaces were reported in the literature by our group in our previous study [26]. It was observed that at all current densities the grain size as observed in FESEM images were in the nanometric range. Also, with the increase in current density, the deposit became coarse and rough, increasing its specific surface area (S2 Supporting Information).

The FESEM images for Fe–Ni-G composite coating deposited from optimal bath at 60 mA cm^{-2} are shown in Fig. 2(a). The addition of graphene to the deposition bath results in the modification of the surface morphology of the coating. The FESEM image shows two different phases on the surface of the coating. The corresponding energy-dispersive X-ray (EDX) spectrum (Fig. 2(d)) indicates that the two phases are irregularly shaped graphene layers embedded with nano-sized Fe–Ni spheres scattered all over the surface of the deposit. Due to the high specific surface area of graphene, the adsorption of electrodeposition solution onto it is expected to be very high. On the application of electric current, the electrolyte adsorbed graphene layers get dragged towards the cathode and gets incorporated into it along with the growing alloy layer. The addition of graphene gives a 3D structure to the deposit (Fig. 2(b)). In addition, due to the high electrical conductivity of graphene, electrodeposition takes place on the surface of embedded graphene. This explains the appearance of nanostructured Fe–Ni alloy spheres on the surface of embedded graphene (Fig. 2(c)). It can be observed from Fig. 2(c) that the Fe–Ni alloy particles are deposited on the graphene surface as nano-sized spheres. The Fe–Ni decorated graphene deposit increases the surface roughness increasing the electroactive surface area of the composite coating. The observation of such structural changes due to the addition of graphene is of great importance in understanding its significance in enhancing the electrocatalytic activity of binary alloy coatings. The appearance of such structures is interesting and advantageous for the purpose of developing 3D surfaces on flat electrodes without sophisticated set up or post treatment such as leaching out one of the metal or etching from metal matrices.

XPS analysis

XPS studies of solid material offer very useful information on elemental composition both on the surface and the bulk of the

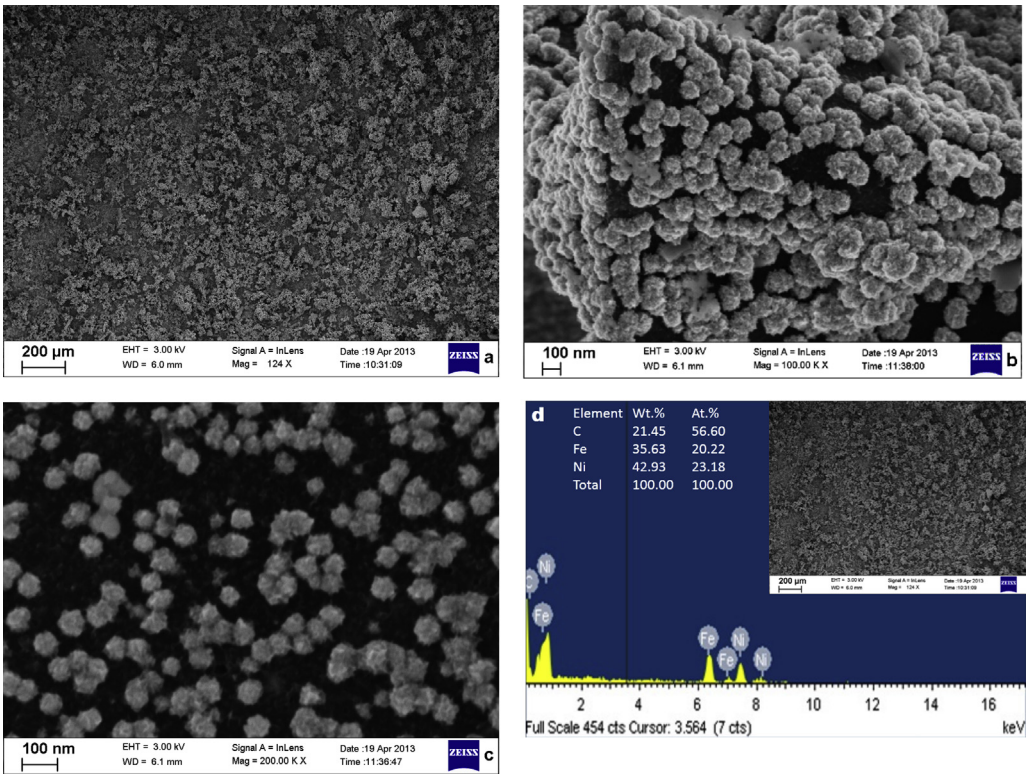

Fig. 2 – FESEM images of (a) Fe–Ni-G composite coating deposited from optimal bath at 60 mA cm^{-2} displaying irregularly shaped graphene layers embedded in Fe–Ni alloy matrix; (b) a magnified image showing the 3D structure encapsulated with nano-sized Fe–Ni spheres on the surface of graphene; (c) magnified image showing nano-sized Fe–Ni spheres decorated on the surface of graphene and (d) EDX spectrum of Fe–Ni-G composite electrode.

sample (up to few layers). Similarly, this technique was used to evaluate the surface deposits, which were obtained galvanostatically at 60 mA cm^{-2}. The wide scan spectrum of Fe–Ni alloy and Fe–Ni-G composite coatings are shown in Fig. 3(a) and (b) respectively. The elemental composition of Fe–Ni alloy and Fe–Ni-G composite coatings are summarized in Table 2.

The deconvoluted C1s spectrum of Fe–Ni alloy coating is as shown in Fig. 4(a). The fitting analysis shows two strong peaks at 285.5 eV corresponding to sp^3 carbon [54] and 290.5 eV corresponding to occluded CO_2 [55]. The sp^3 carbon peak is from ascorbic acid and sodium lauryl sulfate which is added to optimise the bath. The deconvolution of C1s spectrum of Fe–Ni-G composite coating reveals a strong and sharp peak at 284.5 eV corresponding to graphitic sp^2 carbon (Fig. 4(b)) [54,56]. The intensity of sp^3 carbon peak at 285.5 eV is greatly reduced indicating preferential deposition of graphene over amorphous carbon. For similar reasons the intensity of occluded CO_2 peak at 290.5 eV is also reduced.

Fig. 4(c) and (d) shows the core-level Ni2p spectrum for deposits of Fe–Ni alloy and Fe–Ni-G composite coatings respectively. It is possible to identify two species, metallic nickel and nickel oxide as evidenced by peaks at 852.9 eV and 856.0 eV, respectively [57]. From Fig. 4(c) it can be seen that the ratio of peak area, $\left(\frac{A_{Ni(0)}}{A_{Ni(II)}}\right) = 0.36$, indicates an unequal distribution of NiO and Ni metal sites on the surface of Fe–Ni electrode. From Fig. 4(d) it is observed that the ratio of peak area $\left(\frac{A_{Ni(0)}}{A_{Ni(II)}}\right) = 0.95$, indicates almost equal distribution of NiO and Ni metal sites on Fe–Ni-G electrode surface. Similarly in the absence of graphene the core level Fe2p spectrum of Fe–Ni electrode (Fig. 4(e)) shows peaks corresponding to only Fe(II) and Fe(III) [57,58] and does not show any peak corresponding to Fe(0), whereas the core-level Fe2p spectrum of Fe–Ni-G electrode surface (Fig. 4(f)) shows the peak corresponding to Fe(0) [57] with peak area ratios of $\left(\frac{A_{Fe(0)}}{A_{Fe(II)}}\right) = 0.31$ and $\left(\frac{A_{Fe(0)}}{A_{Fe(III)}}\right) = 0.21$.

XRD studies

The phase structure and grain size of the alloy and composite coatings were analysed using XRD technique. The pattern for alloy and composite coatings are plotted to facilitate comparison (Fig. 5). As shown in Fig. 5, the peaks at 2θ values of 43.4°, 50.6° and 74.5° correspond to characteristic peaks of taenite iron–nickel, which could be assigned to (111), (200) and (220) reflection, respectively, of FCC iron–nickel [26,37]. At 60 mA cm^{-2} there was a shift from FCC to BCC phase with appearance of reflection at (110) preferred orientation. The peak of Cu substrate was not observed in the diffraction pattern due to complete coverage of coatings on the surface of the substrate. The coatings at low current density values contain (111) phase as preferred orientation and with the

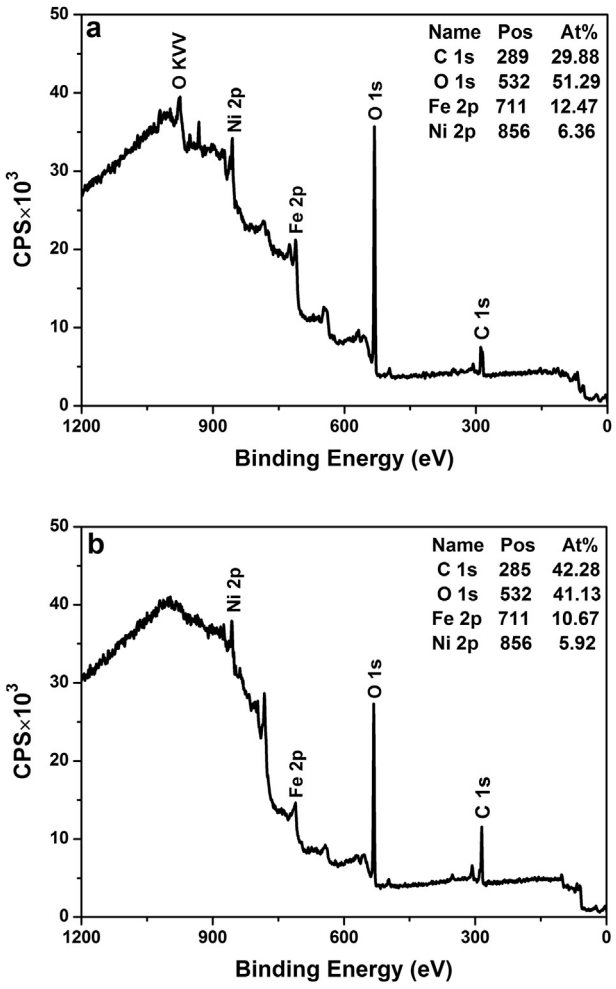

Fig. 3 – Wide scan XPS spectrum of (a) Fe–Ni and (b) Fe–Ni-G.

increase in deposition current density the preferential orientation is more towards (220) phase. All of the XRD patterns clearly show the diffraction peaks of the (400), (422) and (533) crystal planes at 43.2°, 53.5° and 74° respectively, corresponding to the cubic structure of Fe_3O_4 (JCPDS 00-003-0862). The grain size of alloy coatings were calculated using Scherrer equation (Eq. (4)),

$$D = \frac{K\lambda}{\beta\cos\theta} \quad (4)$$

where D is crystallite size, λ is the wavelength of X-ray radiation, β is the full width at half height of symmetrical shape of the diffraction peak and θ is the Bragg angle.

The grain size in the case of alloy and composite coatings is in between 10 and 50 nm and hence deposition at all current densities results in nanocrystalline coatings. On the addition of graphene, the phases of composite coatings appeared unchanged in position but the intensity was slightly on the lower side. Incorporation of graphene into the coating was confirmed by appearance of a low intensity broad peak at 2θ value of 24.5° [59]. The broad peak suggests that the graphene is few layers thick and has a relatively shorter domain size [60]. Other peaks were obtained as in the case of alloy coatings [26].

Table 2 – Elemental composition of Fe–Ni alloy and Fe–Ni-G alloy composite coatings from XPS analysis.

	Fe (at.%)	Ni (at.%)	C (at.%)	O (at.%)
Fe–Ni	12.47	6.36	29.88	51.29
Fe–Ni-G	10.67	5.92	42.28	41.13

Electrochemical characterization

Corrosion study

The corrosion resistance of Fe–Ni alloy coatings were evaluated in the same medium i.e., in 6 M KOH and is reported elsewhere by our group [26]. According to the reported data electrodeposited Fe–Ni alloy coatings under working condition of its electrocatalytic behaviour show least corrosion rate in the range of ~$(1–3) \times 10^{-2}$ mm y^{-1}, well within the tolerable limit for electrode reactions. Hence the corrosion test of electrodeposited Fe–Ni alloy coating qualifies them to be used as safe electrode material for water electrolysis in 6 M KOH as electrolyte.

Hydrogen evolution reaction

The HER of electrolytically coated Fe–Ni-G composite coatings were studied in 6 M KOH solution on 1.0 cm^2 effective geometric surface area. The experiments were performed by cyclic voltammetry and chrono-potentiometry methods and the results are discussed in the following sections.

Cyclic voltammetry study. The electrocatalytic HER in alkaline medium on Fe–Ni-G electrodes were studied by cyclic voltammetry (CV) in a three electrode cell. The experiment was carried out in 6 M KOH electrolyte between −0.5 V and −1.6 V vs. SCE at scan rate of 50 mV s^{-1} for 50 cycles. It was observed in our previous study on Fe–Ni alloy that towards the end of 50^{th} cycle stable and reproducible CV curves were obtained with a state of equilibrium between formation/detachment of hydrogen bubbles (S3 Supporting Information) [26]. Hence CV of Fe–Ni-G composite coatings deposited at different current densities, showing peak cathodic current density (i_{pc}) for HER at the end of 50^{th} cycle is shown in Fig. 6 and corresponding data are given in Table 3. It may be observed that at −1.6 V, i_{pc} for HER increases as the deposition current density increases and is approximately 3 times better than that of binary Fe–Ni alloy coating [26] (S3 Supporting Information), as may be seen in Fig. 7. It may be attributed to the increased electrochemically active surface area of the electrode. It is supported by the increased area covered under the CV plots, as show in Fig. 7.

The FESEM image of Fe–Ni-G composite coating (Fig. 2) shows embedded graphene layers decorated with nano-sized Fe–Ni alloy particles. Thus, the surface roughness of the coating is greatly enhanced by the addition of graphene. This results in increase of electrochemically active surface area and in turn increases the electrocatalytic activity of the composite electrode. Also, XPS analysis reveals that the addition of graphene increases the metallic nickel content in the deposit. The increase in metallic nickel content accelerates the rate determining proton discharge reaction (Volmer reaction) as a result of enhanced charge transfer from Ni(0) to

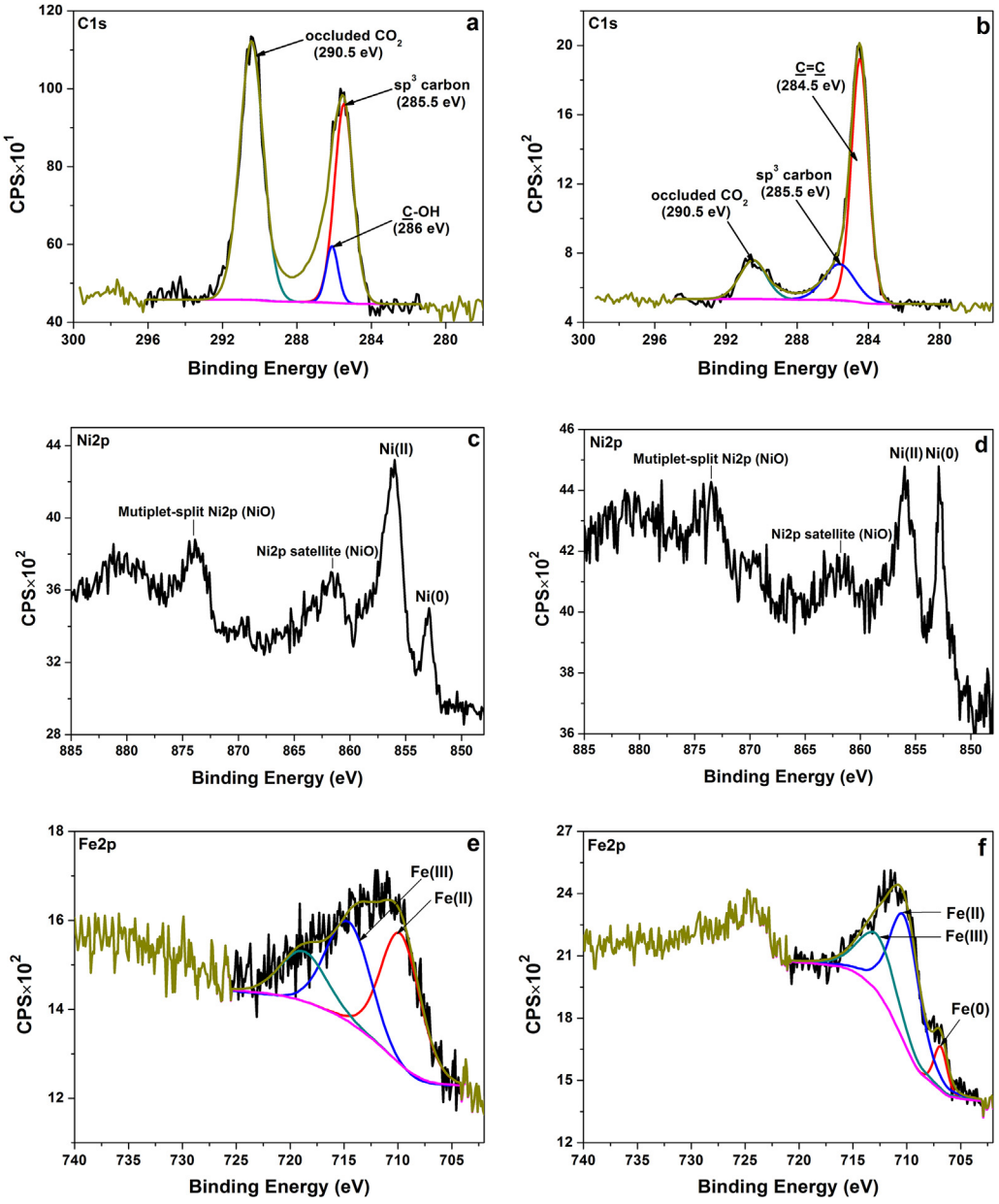

Fig. 4 – XPS core level C1s spectrum of (a) Fe–Ni, (b) Fe–Ni-G; XPS core level Ni2p spectrum of (c) Fe–Ni, (d) Fe–Ni-G and XPS core level Fe2p spectrum of (e) Fe–Ni, (f) Fe–Ni-G.

Fe(0), thereby contributing for increased HER activity of Fe–Ni-G composite electrode [61].

In alkaline media, the HER pathway could be through the Volmer–Tafel (Eqs. (1) and (2)) process or Volmer–Heyrovsky (Eqs. (1) and (3)) pathways. Both pathways involve the adsorption of H_2O molecule, electrochemical reduction of adsorbed H_2O into adsorbed OH^- and H atom, desorption of OH^- to refresh the surface and formation of H adsorbed intermediate for H_2 generation. A pure NiO surface is not active for HER due to the lack of H adsorption sites. On a pure Ni surface without any NiO, the adsorbed OH^- species could occupy the sites for H atom, causing inefficient release of OH^- and blocking of the active catalytic sites. Therefore, for an effective HER catalytic activity, equal distribution of metal oxide and pure metal sites is necessary [51]. As indicated by XPS analysis results, both Ni metal and NiO sites are almost equally distributed in Fe–Ni-G which is responsible for increased HER activity of Fe–Ni-G composite electrode. The ratio of Fe(0) to Fe(II, III) sites in Fe–Ni-G is significant although not equal wherein it too contributes for increased HER activity of Fe–Ni-G composite electrode when compared to Fe–Ni electrode which does not have any Fe(0) sites. The mechanism for the HER activity of Fe(0) in the presence of Fe(II) and Fe(III) is similar to the one proposed for the HER activity of Ni(0) in the presence of Ni(II).

The kinetic behaviour of the electrocatalyst was evaluated by analysing Tafel slope and is shown in Fig. 8. The exchange current densities were calculated by Butler–Volmer equation and the values were in good agreement with values obtained from CV study. In each plot corresponding to different

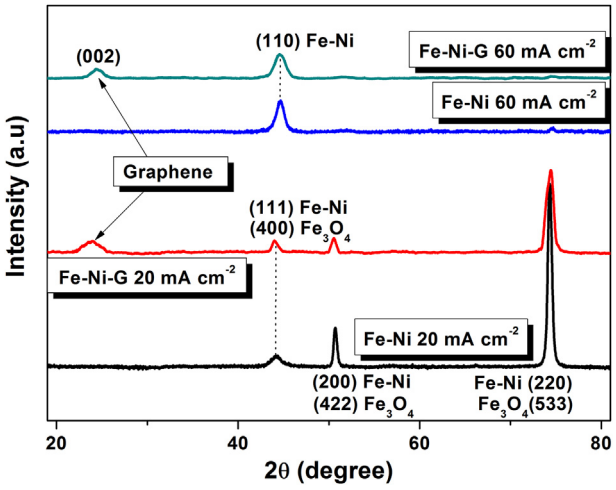

Fig. 5 – XRD patterns of Fe–Ni and Fe–Ni-G coatings demonstrating the significance of deposition current density and graphene on deposit phase structure.

coatings, it may be seen that the first step is an electroreduction of the water molecule, with the formation of hydrogen adsorbed on the electrode surface (Volmer reaction), followed by an electrochemical (Heyrovsky reaction), and/or chemical (Tafel reaction) desorption of H_2. Analysis of the HER mechanism for Fe–Ni and Fe–Ni-G composite coatings have been made based on the Tafel slope (β_c) values [62]. For this analysis, the values of Tafel slope given in the work of Choquette et al. for different HER mechanisms were taken as the reference (up to 66 mV dec^{-1} indicate Heyrovsky–Volmer mechanism; neighbourhood of 118 mV dec^{-1} indicate Volmer–Tafel mechanism and above 200 mV dec^{-1} indicate Tafel mechanism) [63].

Tafel slope (β_c) and exchange current density (i_o) corresponding to Fe–Ni and Fe–Ni-G coatings were determined from Tafel plot (Fig. 8) and the values are reported in Table 4. It may be noted that all the slope values were in the range of −118 mV dec^{-1} confirming that HER on these coatings follow

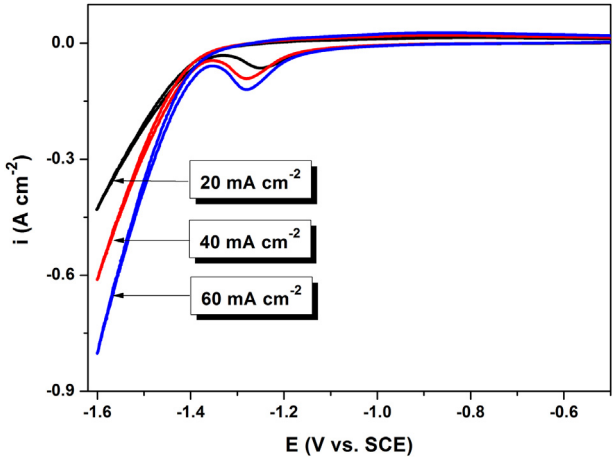

Fig. 6 – CV curves depicting increase of i_{pc} with increase in deposition current density for Fe–Ni-G coatings (on saturation after 50th cycle of CV).

Table 3 – HER parameters for Fe–Ni-G coatings developed at different current densities from optimal bath.

I (mA cm^{-2})	i_{pc} at −1.6 V (A cm^{-2})	Onset potential of H_2 evolution (V vs. SCE)	Volume of H_2 evolved in 300 s (cm^3)
20	0.43	–1.23	12.0
40	0.61	–1.20	13.1
60	0.80	–1.18	14.4

Volmer-Tafel mechanism. There exists an increase of exchange current density for coatings containing graphene indicating that they are more efficient in producing hydrogen on its surface.

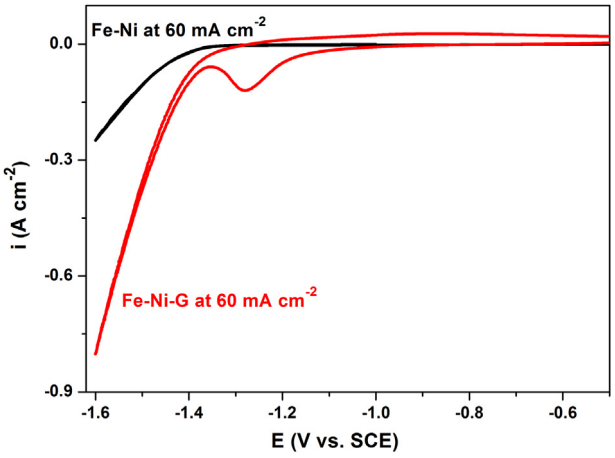

Fig. 7 – Comparison of CV curves for HER on the surface of Fe–Ni and Fe–Ni-G composite coatings (in 6 M KOH electrolyte) deposited at same current density (60 mA cm^{-2}).

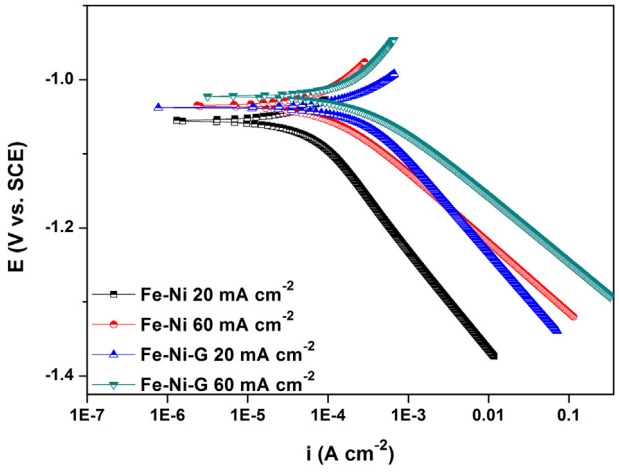

Fig. 8 – Comparison of Tafel slopes (β_c) for HER on electroactive coatings of Fe–Ni and Fe–Ni-G developed under different current densities.

Table 4 – Tafel slope (β_c) and exchange current density (i_o) of Fe–Ni and Fe–Ni-G coatings developed under different current densities.

Electrodeposit coating configuration	Tafel slope, β_c (mV dec^{-1})	i_o (μA cm^{-2})
$(Fe-Ni)_{20\ mA\ cm^{-2}}$	−137.1	53.7
$(Fe-Ni)_{60\ mA\ cm^{-2}}$	−92.6	101.5
$(Fe-Ni-G)_{20\ mA\ cm^{-2}}$	−125.1	132.9
$(Fe-Ni-G)_{60\ mA\ cm^{-2}}$	−88.1	284.5

Chrono-potentiometry. Conventional industrial low-pressure alkaline electrolyzers operate usually at current densities from −100 mA cm^{-2} to −300 mA cm^{-2}. The simplest way to estimate the electrocatalytic activity under these conditions is to monitor the electrode potential at constant current density applied over sufficient period of time by chrono-potentiometry experiment [62]. The chrono-potentiometry study for evolution of hydrogen on Fe–Ni-G composite coatings, deposited at different current densities were made at a constant current density of 300 mA cm^{-2} for a duration of 1500 s. The electrocatalytic behaviour of each coating was evaluated by measuring the amount of H_2 liberated in first 300 s. The nature of chrono-potentiogram for Fe–Ni alloy and Fe–Ni-G composite coating deposited at 60 mA cm^{-2} is shown in Fig. 9. The electrodeposited catalysts showed low potential for HER in the initial period and then the potential slowly stabilized. This phenomenon is ascribed to the formation of hydrogen bubble. The inset chart shows the volume of H_2 liberated in 300 s on each coating deposited at different current density with and without graphene. It may be seen that coating corresponding to 60 mA cm^{-2} shows maximum H_2, due to excess porosity of the coatings. Further, Fe–Ni-G composite coating showed substantial reduction in the hydrogen evolution potential of 170 mV (Table 3) as compared to its binary alloy (Fe–Ni) electrocatalyst (S3 Supporting Information) [26]. Also, the volume of hydrogen gas liberated in 300 s is found to be much higher in the case of composite coatings.

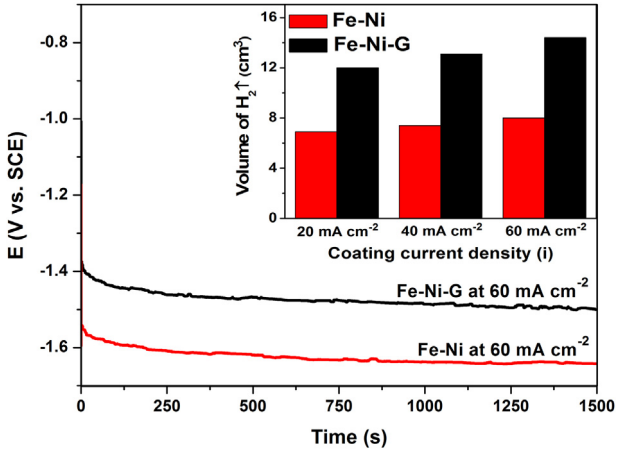

Fig. 9 – Chrono-potentiometry curves at −300 mA cm^{-2} recorded using electroactive coatings of Fe–Ni and Fe–Ni–G deposited at 60 mA cm^{-2}. The inset chart shows the volume of H_2 liberated in 300 s on each coating deposited at different current densities.

Comparison of Fe–Ni-G system with Pt-based materials for HER

When compared to Pt-based materials Fe–Ni-G composite electrode has higher overpotential (approx. −1.2 V) and lower exchange current density [21,49,64–66]. But low abundance, high cost and surface poisoning (e.g. by CO) suggest that Pt-based electrocatalysts cannot be used on a large scale [67–70]. Whereas, Fe–Ni-G composite electrodes does not get easily deactivated by adsorption of poisonous intermediates or reaction products (e.g. CO), thus increasing the active sites for reactant molecules. Unlike Platinum, Fe–Ni-G catalyst combines the ability to oxidize both CO and H_2O effectively [67]. Moreover it is made up of earth-abundant elements and hence is way more economical than Pt-based materials. Also unlike the catalytic reaction on Pt, increasing the concentration of water molecules at the surface favours water-splitting on graphene-based catalysts [71].

Conclusions

In conclusion, we have successfully demonstrated the fabrication of a novel Fe–Ni-G composite electrode for HER by embedding graphene in Fe–Ni alloy matrix via a simple and facile room temperature electrodeposition over copper surface. The addition of graphene to electrolyte bath resulted in porous 3D projections of nano-sized Fe–Ni alloy spheres on the surface of graphene which effectively increases the elelctrochemically active surface area. As indicated by XPS analysis results, both NiO and Ni metal sites are equally distributed in Fe–Ni-G composite electrode. Also the deposition of metallic nickel is favoured on the addition of graphene which accelerates the rate determining proton discharge reaction. All these factors remarkably enhance the HER activity of Fe–Ni-G composite electrode. Under the studied range of current density Fe–Ni-G composite electrode coating developed at 60 mA cm^{-2} was found to be efficient electrode material for HER reaction as demonstrated by cyclic voltammetry and chrono-potentiometry experiments. The Tafel slope analysis shows that the HER follows Volmer-Tafel mechanism.

Acknowledgement

The authors would like to thank Indian Institute of Technology-Bombay and Centre for Nanoscience and Engineering-IISc, Bangalore for providing necessary characterization facilities. BS and YU are grateful to National Institute of Technology Karnataka-Surathkal, for providing financial assistance in the form of Institute fellowship along with necessary facilities and infrastructure to carry out the present work. Special thanks to Dr. David J Morgan, Post-doctoral Research Associate, Cardiff Catalysis Institute, School of Chemistry, Cardiff University and Mr. Rajkamal Balu, PhD Student, Ian Wark Research Institute, University of

South Australia for extending help in the interpretation of XPS results.

Appendix A. Supplementary data

Supplementary data related to this article can be found at http://dx.doi.org/10.1016/j.ijhydene.2015.06.040.

REFERENCES

[1] World Energy Council. World energy scenarios: composing energy futures to 2050. London: World Energy Council; 2013.
[2] Solmaz R, Kardaş G. Electrochemical deposition and characterization of NiFe coatings as electrocatalytic materials for alkaline water electrolysis. Electrochim Acta 2009;54:3726–34.
[3] Turner JA. A realizable renewable energy future. Science 1999;285:687–9.
[4] Dossantosandrade M, Acioli M, Silvajunior J, Silva J, Vilar E, Tonholo J. Preliminary investigation of some commercial alloys for hydrogen evolution in alkaline water electrolysis. Int J Hydrogen Energy 2004;29:235–41.
[5] Turner JA. Sustainable hydrogen production. Science 2004;305:972–4.
[6] Penner SS. Steps toward the hydrogen economy. Energy 2006;31:33–43.
[7] González-Buch C, Herraiz-Cardona I, Ortega E, García-Antón J, Pérez-Herranz V. Synthesis and characterization of macroporous Ni, Co and Ni–Co electrocatalytic deposits for hydrogen evolution reaction in alkaline media. Int J Hydrogen Energy 2013;38:10157–69.
[8] Bocutti R, Saeki MJ, Florentino AO, Oliveira CLF, Ângelo ACD. The hydrogen evolution reaction on codeposited Ni–hydrogen storage intermetallic particles in alkaline medium. Int J Hydrogen Energy 2000;25:1051–8.
[9] Abouatallah RM, Kirk DW, Thorpe SJ, Graydon JW. Reactivation of nickel cathodes by dissolved vanadium species during hydrogen evolution in alkaline media. Electrochim Acta 2001;47:613–21.
[10] Han A, Jin S, Chen H, Ji H, Sun Z, Du P. A robust hydrogen evolution catalyst based on crystalline nickel phosphide nanoflakes on three-dimensional graphene/nickel foam: high performance for electrocatalytic hydrogen production from pH 0–14. J Mater Chem A 2015;3:1941–6.
[11] Vrubel H, Merki D, Hu X. Hydrogen evolution catalyzed by MoS_3 and MoS_2 particles. Energy Environ Sci 2012;5:6136–44.
[12] Voiry D, Yamaguchi H, Li J, Silva R, Alves DCB, Fujita T, et al. Enhanced catalytic activity in strained chemically exfoliated WS_2 nanosheets for hydrogen evolution. Nat Mater 2013;12:850–5.
[13] Safizadeh F, Ghali E, Houlachi G. Electrocatalysis developments for hydrogen evolution reaction in alkaline solutions – a review. Int J Hydrogen Energy 2015;40:256–74.
[14] Kong D, Cha JJ, Wang H, Lee HR, Cui Y. First-row transition metal dichalcogenide catalysts for hydrogen evolution reaction. Energy Environ Sci 2013;6:3553–8.
[15] Kong D, Wang H, Lu Z, Cui Y. $CoSe_2$ nanoparticles grown on carbon fiber paper: an efficient and stable electrocatalyst for hydrogen evolution reaction. J Am Chem Soc 2014;136:4897–900.
[16] Zou X, Zhang Y. Noble metal-free hydrogen evolution catalysts for water splitting. Chem Soc Rev 2015. http://dx.doi.org/10.1039/C4CS00448E.
[17] Pérez-Alonso FJ, Adán C, Rojas S, Peña MA, Fierro JLG. Ni–Co electrodes prepared by electroless-plating deposition. A study of their electrocatalytic activity for the hydrogen and oxygen evolution reactions. Int J Hydrogen Energy 2015;40:51–61.
[18] Domínguez-Crespo MA, Plata-Torres M, Torres-Huerta AM, Ortiz-Rodríguez IA, Ramírez-Rodríguez C, Arce-Estrada EM. Influence of Fe contamination and temperature on mechanically alloyed Co–Ni–Mo electrodes for hydrogen evolution reaction in alkaline water. Mater Charact 2006;56:138–46.
[19] Domínguez-Crespo MA, Plata-Torres M, Torres-Huerta AM, Arce-Estrada EM, Hallen-López JM. Kinetic study of hydrogen evolution reaction on Ni_{30} Mo_{70}, $Co_{30}Mo_{70}$, $Co_{30}Ni_{70}$ and $Co_{10}Ni_{20}Mo_{70}$ alloy electrodes. Mater Charact 2005;55:83–91.
[20] Roué L, Guay D, Schulz R. Hydrogen electrosorption in nanocrystalline Ti-based alloys. J Electroanal Chem 2000;480:64–73.
[21] Metikoš-Huković M, Grubač Z, Radić N, Tonejc A. Sputter deposited nanocrystalline Ni and Ni-W films as catalysts for hydrogen evolution. J Mol Catal A: Chem 2006;249:172–80.
[22] McCandlish LE, Kear BH, Kim BK. Processing and properties of nanostructured WC-Co. Nanostruct Mater 1992;1:119–24.
[23] Ahn SH, Hwang SJ, Yoo SJ, Choi I, Kim H-J, Jang JH, et al. Electrodeposited Ni dendrites with high activity and durability for hydrogen evolution reaction in alkaline water electrolysis. J Mater Chem 2012;22:15153–9.
[24] Ananth MV, Parthasaradhy NV. Hydrogen evolution characteristics of electrodeposited Ni-Zn-Fe coatings in alkaline solutions. Int J Hydrogen Energy 1997;22:747–51.
[25] De Carvalho J, Tremiliosi Filho G, Avaca LA, Gonzalez ER. Electrodeposits of iron and nickel-iron for hydrogen evolution in alkaline solutions. Int J Hydrogen Energy 1989;14:161–5.
[26] Ullal Y, Hegde AC. Electrodeposition and electro-catalytic study of nanocrystalline Ni–Fe alloy. Int J Hydrogen Energy 2014;39:10485–92.
[27] Chang Y-H, Lin C-T, Chen T-Y, Hsu C-L, Lee Y-H, Zhang W, et al. Highly efficient electrocatalytic hydrogen production by MoS_x grown on graphene-protected 3D Ni foams. Adv Mater 2013;25:756–60.
[28] Youn DH, Han S, Kim JY, Kim JY, Park H, Choi SH, et al. Highly active and stable hydrogen evolution electrocatalysts based on molybdenum compounds on carbon nanotube–graphene hybrid support. ACS Nano 2014;8:5164–73.
[29] Łosiewicz B, Budniok A, Rówiński E, Łągiewka E, Lasia A. Effect of heat-treatment on the mechanism and kinetics of the hydrogen evolution reaction on Ni—P + TiO_2 + Ti electrodes. J Appl Electrochem 2004;34:507–16.
[30] Fournier J, Ménard H, Brossard L. Hydrogen evolution reaction on electrocatalytic materials highly dispersed on carbon powder. J Appl Electrochem 1995;25:923–32.
[31] Krstajic N, Trasatti S. Cathodic behaviour of RuO_2-doped Ni/Co_3O_4 electrodes in alkaline solutions: hydrogen evolution. J Appl Electrochem 1998;28:1291–7.
[32] UČ Lačnjevac, Jović BM, Jović VD, Krstajić NV. Determination of kinetic parameters for the hydrogen evolution reaction on the electrodeposited Ni–MoO_2 composite coating in alkaline solution. J Electroanal Chem 2012;677–680:31–40.
[33] Marinović V, Stevanović J, Jugović B, Maksimović M. Hydrogen evolution on Ni/WC composite coatings. J Appl Electrochem 2006;36:1005–9.
[34] Hashimoto K, Sasaki T, Meguro S, Asami K. Nanocrystalline electrodeposited Ni–Mo–C cathodes for hydrogen production. Mat Sci Eng A 2004;375–377:942–5.
[35] Krstajić NV, Gajić-Krstajić L, Lačnjevac U, Jović BM, Mora S, Jović VD. Non-noble metal composite cathodes for hydrogen evolution. Part I: the Ni–MoO_x coatings electrodeposited

from Watt's type bath containing MoO_3 powder particles. Int J Hydrogen Energy 2011;36:6441–9.
[36] Song LJ, Meng HM. Effect of carbon content on Ni–Fe–C electrodes for hydrogen evolution reaction in seawater. Int J Hydrogen Energy 2010;35:10060–6.
[37] Jiang N, Meng H-M, Song L-J, Yu H-Y. Study on Ni–Fe–C cathode for hydrogen evolution from seawater electrolysis. Int J Hydrogen Energy 2010;35:8056–62.
[38] Geim AK, Novoselov KS. The rise of graphene. Nat Mater 2007;6:183–91.
[39] Novoselov KS, Geim AK, Morozov SV, Jiang D, Zhang Y, Dubonos SV, et al. Electric field effect in atomically thin carbon films. Science 2004;306:666–9.
[40] Stoller MD, Park S, Zhu Y, An J, Ruoff RS. Graphene-based ultracapacitors. Nano Lett 2008;8:3498–502.
[41] Chen JH, Ishigami M, Jang C, Hines DR, Fuhrer MS, Williams ED. Printed graphene circuits. Adv Mater 2007;19:3623–7.
[42] Schedin F, Geim AK, Morozov SV, Hill EW, Blake P, Katsnelson MI, et al. Detection of individual gas molecules adsorbed on graphene. Nat Mater 2007;6:652–5.
[43] Eda G, Chhowalla M. Graphene-based composite thin films for electronics. Nano Lett 2009;9:814–8.
[44] Li Q, Guo B, Yu J, Ran J, Zhang B, Yan H, et al. Highly efficient visible-light-driven photocatalytic hydrogen production of CdS-cluster-decorated graphene nanosheets. J Am Chem Soc 2011;133:10878–84.
[45] Subramanya B, Bhat DK. Novel eco-friendly synthesis of graphene directly from graphite using 2,2,6,6-tetramethylpiperidine 1-oxyl and study of its electrochemical properties. J Power Sources 2015;275:90–8.
[46] Subramanya B, Bhat DK. Novel one-pot green synthesis of graphene in aqueous medium under microwave irradiation using a regenerative catalyst and the study of its electrochemical properties. New J Chem 2015;39:420–30.
[47] Suffredini HB, Cerne JL, Crnkovic FC, Machado SAS, Avaca LA. Recent developments in electrode materials for water electrolysis. Int J Hydrogen Energy 2000;25:415–23.
[48] Crnkovic FC, Machado SAS, Avaca LA. Electrochemical and morphological studies of electrodeposited Ni–Fe–Mo–Zn alloys tailored for water electrolysis. Int J Hydrogen Energy 2004;29:249–54.
[49] Lasia A. Hydrogen evolution reaction. Handbook of fuel cells. John Wiley & Sons Ltd; 2010.
[50] Breiter MW. Reaction mechanisms of the H2 oxidation/evolution reaction. Handbook of fuel cells. John Wiley & Sons Ltd; 2010.
[51] Gong M, Zhou W, Tsai M-C, Zhou J, Guan M, Lin M-C, et al. Nanoscale nickel oxide/nickel heterostructures for active hydrogen evolution electrocatalysis. Nat Commun 2014;5:4695.
[52] Zheng Y, Jiao Y, Jaroniec M, Qiao SZ. Advancing the electrochemistry of the hydrogen-evolution reaction through combining experiment and theory. Angew Chem Int Ed 2015;54:52–65.
[53] Jiao Y, Zheng Y, Jaroniec M, Qiao SZ. Design of electrocatalysts for oxygen- and hydrogen-involving energy conversion reactions. Chem Soc Rev 2015;44:2060–86.
[54] Chua CK, Pumera M. Renewal of sp^2 bonds in graphene oxides via dehydrobromination. J Mater Chem 2012;22:23227–31.
[55] Hontoria-Lucas C, López-Peinado AJ, JdD López-González, Rojas-Cervantes ML, Martín-Aranda RM. Study of oxygen-containing groups in a series of graphite oxides: physical and chemical characterization. Carbon 1995;33:1585–92.
[56] Hsiao M-C, Liao S-H, Yen M-Y, Teng C-C, Lee S-H, Pu N-W, et al. Preparation and properties of a graphene reinforced nanocomposite conducting plate. J Mater Chem 2010;20:8496–505.
[57] Sanches LS, Marino CE, Mascaro LH. Characterization of Fe-Ni-W electrodeposits obtained from acid medium. Int J Electrochem Sci 2012;7:9213–20.
[58] Biesinger MC, Payne BP, Grosvenor AP, Lau LWM, Gerson AR, Smart RSC. Resolving surface chemical states in XPS analysis of first row transition metals, oxides and hydroxides: Cr, Mn, Fe, Co and Ni. Appl Surf Sci 2011;257:2717–30.
[59] Kaniyoor A, Baby TT, Ramaprabhu S. Graphene synthesis via hydrogen induced low temperature exfoliation of graphite oxide. J Mater Chem 2010;20:8467.
[60] Eswaraiah V, Jyothirmayee Aravind SS, Ramaprabhu S. Top down method for synthesis of highly conducting graphene by exfoliation of graphite oxide using focused solar radiation. J Mater Chem 2011;21:6800.
[61] Meguro S, Sasaki T, Katagiri H, Habazaki H, Kawashima A, Sakaki T, et al. Electrodeposited Ni-Fe-C cathodes for hydrogen evolution. J Electrochem Soc 2000;147:3003–9.
[62] Tasić GS, Lačnjevac U, Tasić MM, Kaninski MM, Nikolić VM, Žugić DL, et al. Influence of electrodeposition parameters of Ni–W on Ni cathode for alkaline water electrolyser. Int J Hydrogen Energy 2013;38:4291–7.
[63] Choquette Y, Brossard L, Lasia A, Menard H. Study of the kinetics of hydrogen evolution reaction on raney nickel composite-coated electrode by AC impedance technique. J Electrochem Soc 1990;137:1723–30.
[64] Durst J, Siebel A, Simon C, Hasche F, Herranz J, Gasteiger HA. New insights into the electrochemical hydrogen oxidation and evolution reaction mechanism. Energy Environ Sci 2014;7:2255–60.
[65] Markovica NM, Sarraf ST, Gasteiger HA, Ross PN. Hydrogen electrochemistry on platinum low-index single-crystal surfaces in alkaline solution. J Chem Soc Faraday Trans 1996;92:3719–25.
[66] Sheng W, Gasteiger HA, Shao-Horn Y. Hydrogen oxidation and evolution reaction kinetics on platinum: acid vs alkaline electrolytes. J Electrochem Soc 2010;157:B1529–36.
[67] Wolfschmidt H, Paschos O, Stimming U. Hydrogen reactions on nanostructured surfaces. Fuel Cell Science: John Wiley & Sons Inc; 2010. p. 1–70.
[68] Li Q, He R, Gao J-A, Jensen JO, Bjerrum NJ. The CO poisoning effect in PEMFCs operational at temperatures up to 200°C. J Electrochem Soc 2003;150:A1599–605.
[69] Grunes J, Zhu J, Yang M, Somorjai G. CO poisoning of ethylene hydrogenation over Pt catalysts: a comparison of Pt(111) single crystal and Pt nanoparticle activities. Catal Lett 2003;86:157–61.
[70] Su DS, Perathoner S, Centi G. Nanocarbons for the development of advanced catalysts. Chem Rev 2013;113:5782–816.
[71] Boukhvalov DW, Son YW, Ruoff RS. Water splitting over graphene-based catalysts: Ab initio calculations. ACS Catal 2014;4:2016–21.